Journal of Alzheimer's Disease 21 (2010) 1–13
DOI 10.3233/JAD-2010-100159
IOS Press

Familial Alzheimer's Disease Mutations in Presenilins: Effects on Endoplasmic Reticulum Calcium Homeostasis and Correlation with Clinical Phenotypes

Omar Nelson[1], Charlene Supnet, Huarui Liu and Ilya Bezprozvanny*
Department of Physiology, UT Southwestern Medical Center at Dallas, TX, USA

Handling Associate Editor: Jonathan Geiger

Accepted 15 April 2010

Abstract. Mutations in presenilins 1 and 2 (PS1 and PS2) are responsible for approximately 40% of all early onset familial Alzheimer's disease (FAD) monogenic cases. Presenilins (PSs) function as the catalytic subunit of γ-secretase and support cleavage of the amyloid-β protein precursor (AβPP). We previously discovered that PSs also function as passive endoplasmic reticulum (ER) calcium (Ca^{2+}) leak channels and that most FAD mutations in PSs affected their ER Ca^{2+} leak function. To further validate the relevance of our findings to human disease, we here performed Ca^{2+} imaging experiments with lymphoblasts established from FAD patients. We discovered that most FAD mutations in PSs disrupted ER Ca^{2+} leak function and resulted in increased ER Ca^{2+} pool in human lymphoblasts. However, we found that a subset of PS1 FAD mutants supported ER Ca^{2+} leak activity, as ER Ca^{2+} pool was unaffected in lymphoblasts. Most of the "functional" mutations for ER Ca^{2+} leak were clustered in the exon 8–9 area of PSEN1 gene and segregated with the cotton wool plaques and spastic paraparesis clinical phenotype occasionally observed in PS1 FAD patients. Our findings with the "functional" and "non-functional" PS1 FAD mutants were confirmed in Ca^{2+} rescue experiments with PS double-knockout mouse embryonic fibroblasts. Based on the combined effects of the PS1 FAD mutations on ER Ca^{2+} leak and γ-secretase activities we propose a model that explains the heterogeneity observed in FAD. The proposed model has implications for understanding the pathogenesis of both familial and sporadic AD.

Keywords: Alzheimer's disease, amyloid-β, calcium, cotton wool plaques, endoplasmic reticulum, lymphoblasts, presenilins, spastic paraparesis

INTRODUCTION

Alzheimer's disease (AD) is the most common form of age-related dementia in human beings over the age of 60 years. Currently AD affects about 27 million people worldwide and it is speculated that this number will quadruple by 2050. Most cases of AD are idiopathic and characterized by the late onset (> 60 years of age). A small fraction of AD cases (familial AD, FAD) are characterized by an earlier onset and genetic inheritance. The presence of senile plaques and neurofibrillary tangles in the brains of affected individuals are key pathological hallmarks of AD. The plaques contain large amounts of amyloid-β peptide (Aβ) (amyloid plaques) [1,2]. The hyperphosphorylated microtubule

[1]Present address: Department of Molecular and Cellular Pharmacology, University of Miami Miller School of Medicine, Miami, Florida.

*Correspondence to: Dr. Ilya Bezprozvanny, Department of Physiology, ND12.200, UT, Southwestern Medical Center at Dallas Dallas, Texas 75390-9040, USA. Tel.: +1 214 645 6017; Fax: +1 214 645 6018; E-mail: Ilya.Bezprozvanny@UTSouthwestern.edu.

binding protein tau is at the core of the tangles [3]. Mutations in the genes encoding presenilin 1 (PS1), PS2 and amyloid-β protein precursor (AβPP) account for majority of monogenic FAD cases [1,2,4,5]. Mutations in the MAPT gene encoding tau does not lead to AD but instead result in a variant of frontotemporal dementia (FTDP17) [3,6,7]. PSs are 50 kDa proteins that contain 9 transmembrane domains [5,8,9] and resides in the ER membrane [10]. The complex of PS1 or PS2 with Nicastrin, Aph-1, and PEN-2 subunits is transported to the cell surface and functions as γ-secretase, which cleaves the AβPP protein and releases the Aβ peptide, the principal constituent of the amyloid plaques. Consistent with the role of PSs as the catalytic subunits of γ-secretase [5,11,12], FAD mutations in PSs alter AβPP processing to increase the production of the fibrillogenic $A\beta_{42}$ fragment, a finding consistent with the "amyloid hypothesis" of AD pathogenesis [1,2].

Many patients with FAD mutations in PS1 display significant phenotypic heterogeneity [13]. In particular, a subset of PS1-FAD patients manifests symptoms of spastic paraparesis (SP), or progressive spasticity of the lower limbs [5,13–15]. Upon pathological examination of the same patients their brain usually contain abundant large, non-cored plaques, named cotton wool plaques (CWP) composed primarily of $A\beta_{42}$ peptide [5,13–15]. It is believed that accumulation of CWP plaques in basal ganglia, brainstem and spinal cord is responsible for Parkinsonism and spastic phenotypes clinically observed in these patients. Based on initial analysis of 3 different CWP PS1-FAD mutations, it has been suggested that these mutations cause very large increase in $A\beta_{42}$ production [16]. However, it was later discovered that other CWP-linked PS-FAD mutations do not have such large effects on $A\beta_{42}$ production. Thus, the reasons for unique clinical and pathological phenotypes observed in these PS1-FAD pedigrees remain poorly understood [5,13–15].

In addition to the "amyloid hypothesis", a "Ca^{2+} hypothesis" of AD pathogenesis has been previously proposed. The "Ca^{2+} hypothesis of AD" states that deranged Ca^{2+} signaling plays an important role in AD pathogenesis [17,18]. Interestingly, many FAD mutations in PSs result in deranged Ca^{2+} signaling (reviewed in [18,19]). Although the connection between FAD mutations in PSs and abnormal Ca^{2+} signaling has been known for over a decade [20], the mechanistic explanation for these findings has been lacking until recently. As a potential explanation for these results we recently proposed that PSs function as passive ER Ca^{2+} leak channels [21]. Moreover, we discovered that a number of FAD mutations in PSs abolished their ER Ca^{2+} channel function [21,22]. In order to further expand and authenticate our findings, we here performed analysis of ER Ca^{2+} leak function in cells from a number of additional FAD mutants in PS1. In parallel experiments we also evaluated Ca^{2+} signals in cells established from patients with FAD mutation in AβPP, FTDP17 mutation in tau and from AD patients with unidentified genetic mutations. From these results we concluded that FAD mutations in PSs specifically affected their ER Ca^{2+} leak activity. We also discovered that a subset of PS1 FAD mutants supported ER Ca^{2+} leak activity. Most of the functional mutations for ER Ca^{2+} leak were clustered in exon 8-9 area of PSEN1 gene and segregated with the CWP/SP clinical phenotypes. The obtained results provide novel insights into potential role of the ER Ca^{2+} leak pathway in AD pathogenesis.

MATERIALS AND METHODS

Human lymphoblast cell lines

The human lymphoblasts cell lines were obtained from the National Cell Repository for Alzheimer's disease (NCRAD). The following lines were obtained from NCRAD: healthy donor (WT), PS1-M139V, PS1-M146L, PS1-K239E, PS1-V261F, PS1-P264L, PS1-R269G, PS1-C410Y, PS1-A426P, PS1-A431E, PS1-ΔE9, PS2-N141I, tau-R406W, AβPP-V717L, OAD (age of onset: 68, negative for PSEN1 mutations; PSEN2 gene not tested; negative for AβPP mutations), YAD1 (age of onset 47, negative for PSEN1 mutations; PSEN2 not tested; negative for AβPP mutations) and YAD2 (age of onset 43, negative for PSEN1 mutations, but polymorphism (T/G) at +16 outside Exon 9 of PSEN1 was noted; PSEN2 and AβPP genes not tested). Standard lymphoblast culture procedures were used. Lymphoblasts were maintained in suspension culture in RPMI 1640 medium (Sigma Chemical Co.) supplemented with 10% fetal bovine serum (FBS) (Gemini), 100 μg/ml streptomycin and 100 U/ml penicillin (Sigma Chemical Co.) at 37°C in an atmosphere of 5% CO_2/95% air.

Ca^{2+} flux measurements

For Ca^{2+} flux measurements the lymphoblasts were transferred to HCSS buffer (120 mM NaCl, 5.4 mM KCl, 0.8 mM $MgCl_2$, 2 mM $CaCl_2$, 15 mM glucose,

and 20 mM HEPES, pH 7.3) and loaded with 3 μM Fura2-AM (Molecular Probes) for 45 min at 37 °C. The cells were then washed with HCSS buffer by centrifugation and resuspended in HCSS-Ca^{2+} deficient buffer (buffered with EGTA to 170 nM Ca^{2+}) immediately prior to Ca^{2+} imaging experiments. The Ca^{2+} measurements were performed with 1.8 ml of cell suspension (1×10^6 cells) in a 2 ml quartz cuvette using the Felix system (Photon Technology International, PTI). The suspension of the cells loaded with Fura-2 was challenged with 5 μM ionomycin and the increase in Fura-2 340/380 cytosolic ratio signals was measured over time. At the end of each experiment, the 340/380 Fura-2 ratios were calibrated by consecutive additions of 10 μM ionomycin, 2 mM $CaCl_2$, and 20 mM EGTA. The 340/380 Fura-2 ratios were converted to free Ca^{2+} concentration in the cuvette by using the equation from [23]. The size of ER Ca^{2+} pool was calculated by integrating the amount of Ca^{2+} released from the stores following addition of 5 μM ionomycin.

PS1 expression constructs

The L85P, M139V, G217D, V261F, P264L, E280G, T291P, C410Y, N405S, L420R, A426P, and A431E mutations in wild type PS1 cloned into pcDNA3 expression vector were generated by Quick-change site-directed mutagenesis kit (Stratagene) and verified by sequencing. PS1-ΔE8 construct was provided by Sam Gandy (Mount Sinai School of Medicine, NYC) [24] and recloned into pcDNA3.

Ca^{2+} imaging experiments PS-DKO MEF cells

The PS double-knockout (DKO) mouse embryonic fibroblasts (MEF) cells were previously described [25, 26]. Ca^{2+} imaging experiments with MEFs were performed as previously described [21,22]. Briefly, PS DKO cells were transfected using Lipofectamine (Invitrogen) by pEGFP-C3 plasmid (Clontech) or by a 1:3 mixture of pEGFP-C3 and PS1-expression plasmids. The Ca^{2+} imaging experiments were performed 48 h after transfection. The cells were cultured on poly-D-lysine (Sigma) coated 12 mm round glass coverslips and loaded with 5 μM Fura-2-AM (Molecular Probes) in HCSS buffer (120 mM NaCl, 5.4 mM KCl, 0.8 mM $MgCl_2$, 2 mM $CaCl_2$, 15 mM glucose, and 20 mM HEPES, pH 7.3) for 45 min at 37°C. For Ca^{2+} imaging experiments the coverslips were mounted onto a recording/perfusion chamber (RC-26G, Warner Instrument), positioned on a movable stage of an Olympus IX-70 inverted microscope and washed with HCSS-Ca^{2+} deficient buffer (buffered with EGTA to 50 nM Ca^{2+}). The transfected cells were identified by GFP imaging using GFP filter cube (Chroma) as we previously described [21,22]. In Ca^{2+} imaging experiments the cells were intermittently excited by 340 nm and 380 nm UV light (DeltaRam illuminator, PTI) using a Fura-2 dichromic filter cube (Chroma Technologies) and 60 × UV-grade oil-immersed objective (Olympus). The emitted light was collected by an IC-300 camera (PTI), and the images were digitized by the ImageMaster Pro software (PTI). Baseline (6 min) measurements were obtained prior to bath application of drugs. The drugs: 300 nM Bradykinin (BK) and 5 μM ionomycin (IO) (both from Sigma) were dissolved in HCSS-Ca^{2+} deficient buffer prior to application to the cells. Images at 340 nm and 380 nm excitation wavelengths were captured every 2 s and shown as 340/380 image ratios at time points as indicated. Background fluorescence was determined according to manufacturer's (PTI) recommendations and subtracted. The absolute values of free cytosolic Ca^{2+} concentrations ($[Ca^{2+}]$) in these experiments were determined from the equation [23].

$$[Ca^{2+}] = K_d \quad \frac{[R - R_{\min}]}{R_{\max} - R} \frac{S_{f,380}}{S_{b,380}}$$

where $K_d = 140$ nM is the affinity of Fura-2 for Ca^{2+}, R is the experimentally determined 340/380 ratio, R_{max} is the 340/380 ratio for Fura-2 saturated with Ca^{2+} (determined by application of 20 mM Ca^{2+} and 10 μM ionomycin at the end of the experiment), R_{min} is the 340/380 ratio for Ca^{2+}-free Fura-2 (determined by addition of 20 mM EGTA following R_{max} determination), and $s_{f,380}/s_{b,380}$ is the ratio of fluorescence intensity of Ca^{2+}-free and Ca^{2+}-bound form of Fura-2 at 380 nM ($s_{f,380}/s_{b,380} = 2$ in our experiments).

Statistical analysis

All data were subjected to one-way ANOVA analysis, and the changes were considered statistically significant at $p < 0.05$ cutoff value.

RESULTS

Ca^{2+} signaling defects In human FAD lymphoblasts

Our previous studies [21,22] were preformed with recombinant PSs reconstituted into planar lipid bilayers or expressed in the MEF cells. Based on these

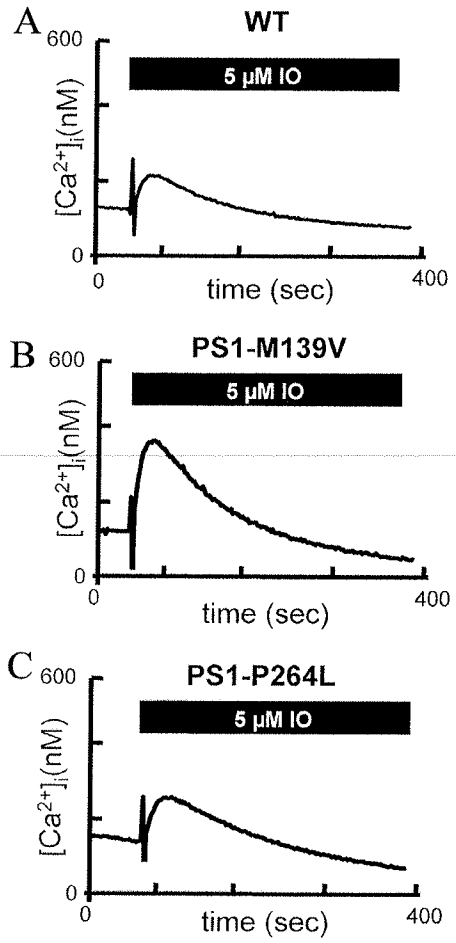

Fig. 1. Ca^{2+} signals in lympoblast from the FAD patient. A) The time course of ionomycin(IO)-induced Ca^{2+} signals in representative experiments with wild type lymphoblast. B) The time course of ionomycin(IO)-induced Ca^{2+} signals in representative experiments with lymphoblast from FAD patient harboring PS1-M139V mutation. C) The time course of ionomycin(IO)-induced Ca^{2+} signals in representative experiments with lymphoblast from FAD patient harboring PS1-P264L mutation.

results we concluded that both PS1 and PS2 holoproteins function as passive ER Ca^{2+} leak channels and that most FAD mutations in presenilins abolished their ER Ca^{2+} leak channel activity. To further establish the relevance of our findings for human disease, we obtained a collection of lymphobasts from FAD patients harboring PS mutations from the National Cell Repository for Alzheimer's disease (NCRAD). In addition, we also obtained lymphobasts from patients with point mutations in tau and AβPP proteins and from AD patients with unidentified genetic mutations. We also obtained lymphoblasts from healthy donors. To evaluate the ER Ca^{2+} pool in collected cells the lymphoblasts were loaded with the cytosolic Ca^{2+} imaging dye Fura-2. The suspension of the cells (1×10^6 cells) was placed to a quartz cuvette in a Ca^{2+}-free media and challenged with 5 μM of the Ca^{2+} ionophore ionomycin (IO). We discovered that application of ionomycin induced modest Ca^{2+} response in lymphoblasts from control healthy individuals (WT) (Fig. 1A). In contrast, application of ionomycin induced significantly larger responses in lymphoblasts from FAD patients harboring PS1-M139V mutation (Fig. 1B). To quantify the IO-sensitive Ca^{2+} pool in these cells, we converted Fura-2 Ca^{2+} signals into cytosolic Ca^{2+} concentration values and integrated an area under IO-induced Ca^{2+} response curves (Fig. 1) for each type of cells. We found that on average the size of the IO-sensitive Ca^{2+} pool was equal to 11 ± 3 μM·sec ($n = 15$) for WT lymphoblasts (Fig. 2). The average of the IO-sensitive Ca^{2+} pool in PS1-M139V lymphoblasts was equal to 19 ± 4 μM·sec ($n = 9$), significantly higher than in WT lymphoblasts (Fig. 2). The results obtained with PS1-M139V lymphoblasts are in agreement with our previous findings that many FAD mutations in PSs impaired ER Ca^{2+} leak function and increased the IO-sensitive Ca^{2+} pool in cells [21,22]. However, when lymphoblasts from FAD patients harboring PS1-P264L mutation were tested in the Ca^{2+} flux assay, the IO-induced Ca^{2+} response was similar to the response in WT cells (Fig. 1C). An average IO-sensitive Ca^{2+} pool in PS1-P264L cells was equal to 9 ± 2 μM·sec ($n = 9$), not significantly different from the WT cells (Fig. 2). Thus, we concluded that some but not all PS-FAD lymphoblasts have impaired ER Ca^{2+} leak function and increased ER Ca^{2+} pool.

To systematically evaluate the ER Ca^{2+} pool in AD cells, we performed Ca^{2+} flux measurements with all FAD lymphoblasts received from NCRAD. When compared with the cells from healthy donor (WT), we determined that the IO-sensitive Ca^{2+} pool was significantly elevated in FAD lymphoblasts harboring PS1 mutations M139V, M146L, K239E, V261F, A431E and PS2 mutation N141I (Fig. 2). We previously reported that PS1-M146L and PS2-N141I mutations abolish ER Ca^{2+} leak function of PSs [21]. An increase in the IO-sensitive Ca^{2+} pool in PS1-M146L and PS2-N141I lymphoblasts (Fig. 2) is consistent with our previous findings. Our new results (Fig. 2) suggest that M139V, K239E, V261F, and A431E FAD mutations also impair ER Ca^{2+} leak function of PS1. In contrast to these mutations, the IO-sensitive Ca^{2+} pool was not significant-

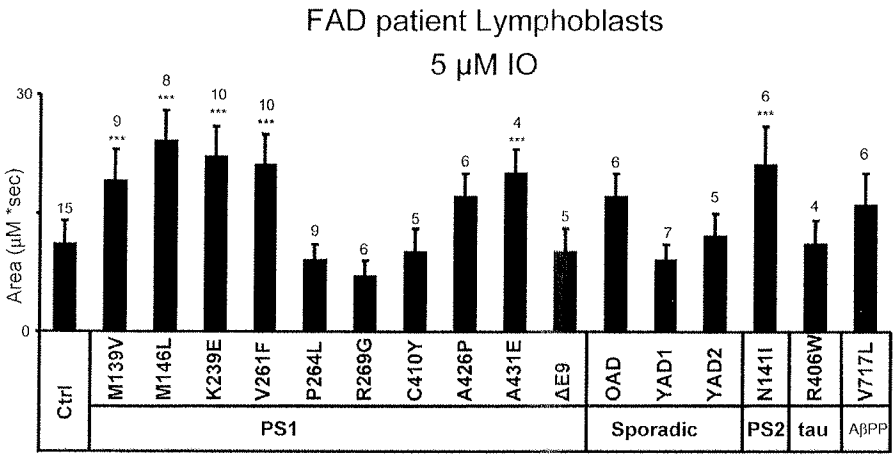

Fig. 2. Ca^{2+} signals in human lymphoblast from FAD patients. The average size of ionomycin (IO)-releasable Ca^{2+} pool is shown for human FAD lymphoblast data is shown as mean ± S.D. (n = number of experiments done). When compared to WT lymphoblast, the size of IO-releasable Ca^{2+} pool is significantly (***$p < 0.05$ by ANOVA) larger in FAD lymphoblast with PS1 mutation M139V, M146L, K239E, V261F, A431E, and PS2-N141I. There were no significant differences in the IO-releasable Ca^{2+} pool of PS1-P264L, R269G, C410Y, A426P, ΔE9, tau-R406W, APP-V717L, young (YAD), or old (OAD) sporadic cases when compared to WT. Even though the IO-releasable Ca^{2+} pool was more elevated in FAD lymphoblast PS1-A426P, APP-V717L and OAD there were no significant difference compared to WT lymphoblast.

ly elevated in FAD lymphoblasts harboring PS1 mutations P264L, R269G, C410Y, and ΔE9 (Fig. 2). We previously reported that PS1-ΔE9 mutants was able to function as an ER Ca^{2+} leak channel [21]. The results obtained with PS1-ΔE9 lymphoblasts are consistent with our previous findings (Fig. 2). It appeared that PS1-FAD mutations P264L, R269G, C410Y also correspond to functional ER Ca^{2+} leak channels (Fig. 2). The IO-sensitive Ca^{2+} pool was elevated in PS1-A426P lymphoblasts, but were not statistically different than WT at $p = 0.05$ cutoff (Fig. 2). It was not clear from the obtained results if PS1-A426P mutation causes impaired ER Ca^{2+} leak function or not (Fig. 2).

The size of the IO-sensitive Ca^{2+} pool was not increased in lymphoblasts from the FTDP17 patient harboring tau-R406W mutation or from the AD patients YAD1 (age on onset 47) and YAD2 (age of onset 43) (Fig. 2). There was some increase in the IO-sensitive Ca^{2+} pool in OAD patient (age of onset 68) and from FAD patient harboring AβPP-V717L mutation (Fig. 2). However, in both of these cases the differences did not reach statistical significance at $p = 0.05$ cutoff compared to WT (Fig. 2). Based on these results we concluded that ER Ca^{2+} signaling is specifically disrupted in lymphoblasts from the patients with FAD mutations in PSs (Fig. 2). Thus, for the remainder of the study we focused on the analysis of ER Ca^{2+} leak function of PS1-FAD mutations.

Rescue of Ca^{2+} signaling defects in PS DKO MEFs with FAD PS1 mutants

Experiments with lymphoblasts from FAD patients suggest that some PS1-FAD mutations disrupt ER Ca^{2+} homeostasis and some do not (Fig. 2). These data are consistent with our previous findings that PS1-M146V and PS2-N141I mutations disrupt ER Ca^{2+} leak function of PSs, whereas PS1-ΔE9 mutant is able to function as ER Ca^{2+} leak channels [21,22]. To test these conclusions for the remaining PS1-FAD mutants we performed a series of Ca^{2+} rescue experiments with PS DKO MEF cells. As in previous studies [21,22], the PS DKO MEF cells were co-transfected with PS1-FAD mutant constructs and pEGFP plasmid, and Ca^{2+} imaging experiments were performed on GFP-positive cells 48h after transfection. In control experiments, PS DKO MEF cells were transfected with pEGFP plasmid alone or co-transfected with WT PS1 construct. We found that for EGFP-transfected DKO cells the average basal Ca^{2+} level was equal to 173 ± 32 nM ($n = 56$) (Fig. 3A, gray bar), the average amplitude of BK-induced Ca^{2+} response was equal to 693 ± 93 nM ($n = 37$) (Fig. 3A, black bar) and the average IO-sensitive Ca^{2+} pool was equal to 50 ± 9 μM·sec ($n = 33$) (Fig. 3B). Expression of wild type human PS1 construct in PS DKO cells increased the basal cytosolic Ca^{2+} levels to 257 ± 39 nM ($n = 61$) (Fig. 3A, gray bar), reduced the amplitude of BK-induced Ca^{2+} response to 221 ± 36 nM

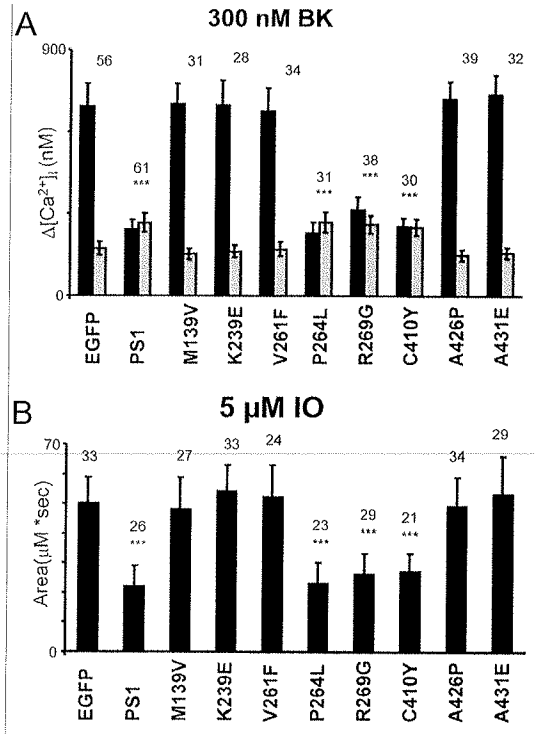

Fig. 3. Summary of PS1-FAD rescue experiments. A) The average basal cytosolic Ca^{2+} levels (gray bars) and amplitude of BK-induced Ca^{2+} responses (black bar) is shown for DKO cells transfected with EGFP and PS1 expression constructs as mean ± S.D. (n = number of cells analyzed). When compared to DKO cells transfected with EGFP alone, the basal Ca^{2+} levels are significantly higher (***$p < 0.05$ by ANOVA) and the amplitude of BK-induced Ca^{2+} response is significantly smaller (***$p < 0.05$ by ANOVA) in DKO cells transfected with EGFP + PS1, EGFP + PS1-P264L, EGFP+ PS1-R269G and EGFP + C410Y combinations. There were no differences between EGFP alone and the PS1 mutations (M139V, K239E, V261F, A426P, and A431E). B) The average size of ionomycin (IO)-releasable Ca^{2+} pool is shown for DKO cells transfected with EGFP and PS1 expression constructs is shown as mean ± S.D. (n = number of cells analyzed). When compared to DKO cells transfected with EGFP alone, the size of IO-releasable Ca^{2+} pool is significantly (***$p < 0.05$ by ANOVA) smaller in DKO cells transfected with EGFP + PS1 and EGFP + PS1-P264L, EGFP+PS1-R269G and EGFP + C410Y combinations when compared to DKO cells transfected with EGFP plasmid alone.

($n = 37$) (Fig. 3A, black bar) and reduced the size of IO-sensitive Ca^{2+} pool to 22 ± 7 μM·sec ($n = 26$) (Fig. 3B). All three parameters were significantly ($p < 0.05$) different in DKO cells co-transfected with EGFP and wild type PS1 construct when compared to DKO cells transfected with EGFP plasmid alone (Figs 3A, 3B). These findings are in quantitative and qualitative agreement with our previous results [21,22]. As we argued previously, these results can be explained by an ability of over-expressed wild type PS1 to rescue ER Ca^{2+} leak pathway deficiency in PS DKO MEF cells.

In rescue experiments with PS1-FAD mutants, we found that transfection of P264L, R269G, and C410Y PS1 mutant had the same effects on the basal cytosolic Ca^{2+} levels, the amplitude of BK-induced Ca^{2+} response, and the size of IO-sensitive Ca^{2+} pool as transfection of WT PS1 construct (Figs 3A, 3B). Thus, we concluded that P264L, R269G, and C410Y PS1-FAD mutants maintain their ability to function as ER Ca^{2+} leak channels. In contrast, expression of M139V, K239E, V261F, A426P, and A431E PS1-FAD mutants had no significant effect on any of these three parameters when compared to transfection with control EGFP plasmid (Figs 3A, 3B). From these results we concluded that M139V, K239E, V261F, A426P, and A431E PS1-FAD mutants lost their ability to function as ER Ca^{2+} leak channels. These results are in near perfect agreement with predictions made on the basis of Ca^{2+} flux measurements with human FAD patient lymphoblasts (Fig. 2). The only difference is the PS1-A426P mutant, which resulted only in a partial increase in the size of IO-sensitive Ca^{2+} pool in lymphoblasts (Fig. 2) but appeared to be complete loss of function mutant in PS DKO MEF rescue experiments (Fig. 3). A reasonable explanation of the discrepancy is the fact that FAD patient lymphoblasts have been obtained from patients who are heterozygous for the mutation. As a result, effects on Ca^{2+} signaling are expected to be attenuated in patient lymphoblasts when compared to PS DKO MEF rescue experiments.

CWP/SP PS1 FAD mutations and ER Ca^{2+} leak function

Senile plaques composed of aggregated Aβ peptide is a key pathological hallmark of AD. Typically these plaques are known as dense core plaques (DCP) and are associated with dystrophic neurites, degenerating neurons and inflammatory pathology. The rare variant CWPs consist of large round Aβ deposits primarily positive for Aβ_{42} peptide [27]. The CWPs are devoid of a compact amyloid core and lack surrounding neuritic pathology [28,29]. PS1-FAD patients with CWP pathology often display the SP clinical phenotype, and are classified as CWP/SP FAD cases [13–15]. If the ER Ca^{2+} leak function of presenilins has some relevance for AD pathogenesis, one can expect that "functional" and "non-functional" PS1-FAD mutants may result in the different clinical representations of the disease.

Table 1

PS Ca^{2+} Leak Function and PS-FAD Clinical and Pathological Phenotypes. The summary of results obtained in the present study and the previous publications [21,22] is shown. The mutations are divided into loss of ER Ca^{2+} leak function (LOF) and "functional" groups. The position of each mutation in PSEN1 gene and in PS1 structural domains is indicated. Also shown are the effects on ER Ca^{2+} leak function, mean age of disease onset for patients with the corresponding mutation, published $A\beta42/A\beta40$ ratios, reported clinical phenotypes and plaque pathology. Clinical phenotypes and $A\beta42/A\beta40$ ratios are compiled from [13–15], original literature and http://www.molgen.ua.ac.be/ADMutations [43]. Clinical features: myoclonus (Myo), Seizures (Sei), Extrapyramydal signs (EPS), Behavioral and psychiatric features (BPS), Frontotemporal dementia (FTD), Spastic paraparesis (SP), Cerebellar ataxia (CA), dilated cardiomyopathy (DCM). Pathology: dense core plaques (DCP), cotton wool plaques (CWP), amyloid angiopathy (AA). ND – not determined

PS-FAD	Exon	Domain	Calcium leak function	Mean age onset	$A\beta_{42}/A\beta_{40}$	Clinical phenotype	plaque pathology
			LOF				
M139V	EX5	TM2	LOF	41	1.9x ↑	Myo, Sei, EPS, CA,	DCP
M146V/I/L	EX5	TM2	LOF	38	2.0x ↑	Myo, Sei, EPS, Apraxia	DCP
L166P	EX6	TM3	LOF	24	7.6x ↑	SP, Sei, BPS, CA	CWP
G217D	EX7	HL4	LOF	40	ND	EPS, Parkinsonism	CWP, AA
K239E	EX7	HL5	LOF	58	ND	Unpublished (NRCAD)	
A246E	EX7	TM6	LOF	52	2.4x ↑		DCP
V261F	EX8	TM6	LOF	36	ND	SP	CWP
E273A	EX8	HL6a	LOF	63	ND		
G384A	EX11	TM7	LOF	35	8.0x ↑		
L420R	EX12	TM8	LOF	38	ND	Seizures	CWP
A426P	EX12	TM8	LOF	46	ND		
A431E	EX12	HL8	LOF	40	ND	EPS, aphasia, spasticity	
P436Q	EX12	TM9	LOF	28	4.3x ↑	SP	CWP
PS2-N141I		TM2	LOF	60	6.2x ↑		
			Functional				
A79V	EX4	N-term	functional	61	1.8x ↑	Partial penetrance	
L85P	EX4	TM1	functional	26	1.9x ↑	SP, visual impairment	
P264L	EX8	HL6a	functional	46	1.3x ↑	SP, Sei, Myo, Atypical Dementia	CWP
R269G	EX8	HL6a	functional	49	ND	Sei, Myo	
ΔE8/D257A (L271V)	ΔEX8	TM6-HL6a	functional	49	1.4x ↑		CWP, AA
E280G	EX8	HL6 (MA)	functional	45	1.5x ↑	SP	CWP, AA
ΔE9/S290C	ΔEX9	HL6 (MA)	functional (GOF)	45	4.8x ↑	SP, BPS	CWP
T291P	EX9	HL6 (MA)	functional	33	1.6x ↑	SP	CWP
N405S	EX11	HL7	functional	48	ND	SP	CWP
C410Y	EX11	TM8	functional	50	1.8x ↑	Parkinsonism	CWP
			FTD-implicated				
L113P	EX4	HL1	functional	39	ND	BPS, Sei, Myo, EPS, FTD	
G183V	EX6	HL3	functional	51	1.5x ↑	BPS, FTD	Pick
Rins352	EX10	HL6b	functional	56	ND	BPS, FTD. Not pathogenic.	

We searched for such a correlation and discovered that the majority of "functional" PS1-FAD mutants have been linked with the CWP/SP phenotype in AD patients. These mutations are PS1-ΔE9 (CWP/SP) [28, 29], P264L (CWP/SP) [30] and C410Y (CWP, Parkinsonism) [31] (Table 1).

To test this correlation further, we performed Ca^{2+} imaging experiments with PS DKO MEF cells transfected with several additional CWP/SP PS1-FAD mutant constructs. The CWP/SP PS1 mutants for these studies were identified by literature search and then generated by site-directed mutagenesis. The PS1-FAD constructs selected for these experiments were: L85P (SP, plaque pathology unknown) [32], G217D (CWP, Parkinsonism) [33], ΔE8 (CWP) [24], E280G (CWP/SP) [34,35], T291P (CWP/SP) [36], N405S (CWP/SP) [37], and L420R (CWP) [38]. As in previous experiments [21,22], the constructs were co-transfected with EGFP expression plasmid and WT PS1 construct was used as a positive control. The steady-state basal Ca^{2+} levels, the amplitude of BK-induced Ca^{2+} response, and the IO-sensitive Ca^{2+} pool was measured in GFP-positive cells 48h after transfection as described in the previous section. In these experiments we discovered that expression of L85P, ΔE8, E280G, T291P, and N405S PS1-FAD mutants in PS DKO MEF cells increased the basal Ca^{2+} levels (Fig. 4A, grey bars), reduced the amplitude of BK-induced Ca^{2+} responses (Fig. 4A, black bars), and reduced the IO-sensitive Ca^{2+} pool (Fig. 4B). Thus, we concluded that all these mutants encode functional ER Ca^{2+} leak channels (Table 1). In contrast, G217D and L420R PS1-FAD mutants were not able to rescue any of the Ca^{2+} signaling defects in PS DKO MEF cells (Figs 4A, 4B)

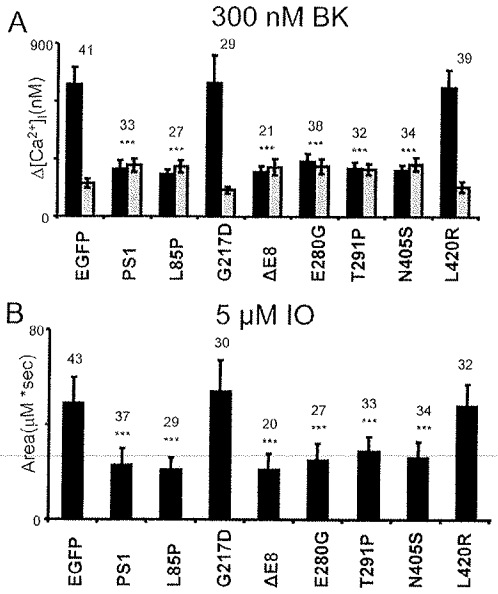

Fig. 4. Summary of CWP PS1-associated rescue experiments. A) The average basal cytosolic Ca^{2+} levels (gray bars) and amplitude of BK-induced Ca^{2+} responses (black bar) is shown for DKO cells transfected with EGFP and PS1 expression constructs as mean ± S.D. (n = number of cells analyzed). When compared to DKO cells transfected with EGFP alone, the basal Ca^{2+} levels are significantly higher (***$p < 0.05$ by ANOVA) and the amplitude of BK-induced Ca^{2+} response is significantly smaller (***$p < 0.05$ by ANOVA) in DKO cells transfected with EGFP + PS1, EGFP +PS1-P85L, EGFP +PS1-P264L, EGFP + PS1-E280G, EGFP +PS1-P284H, EGFP+ PS1-T291P, EGFP +PS1-N405S, and EGFP + ΔE8 combinations. There was no significant difference with EGFP alone compared to EGFP +PS1-G217D and EGFP +PS1-L420R. B) The average size of ionomycin (IO)-releasable Ca^{2+} pool is shown for DKO cells transfected with EGFP and PS1 expression constructs is shown as mean ± S.D. (n = number of cells analyzed). When compared to DKO cells transfected with EGFP alone, the size of IO-releasable Ca^{2+} pool is significantly (***$p < 0.05$ by ANOVA) smaller in DKO cells transfected with EGFP + PS1 and EGFP +PS1-P85L, EGFP +PS1-E280G, EGFP +PS1-P284H, EGFP+ PS1-T291P, EGFP +PS1-N405S, and EGFP + ΔE8 combinations when compared to DKO cells transfected with EGFP plasmid alone. There was no significant difference with EGFP alone compared to EGFP +PS1-G217D and EGFP +PS1-L420R.

and we concluded that these two mutants were "loss of function" for ER Ca^{2+} leak activity (Table 1). From this analysis we concluded that the majority of CWP/SP PS1-FAD mutants are indeed functional in ER Ca^{2+} leak assay, but that a few exceptions also exist.

DISCUSSION

Based on results obtained in our previous studies [21, 22] we concluded that the PS1 and PS2 holoproteins function as passive ER Ca^{2+} leak channels and that most FAD mutations in PSs abolished their ER Ca^{2+} leak channel activity. Results obtained in the current study enable us to further extend and clarify our previous conclusions. We now confirmed that ER Ca^{2+} stores are overloaded in lymphoblasts established from FAD patients with mutations in presenilins (Figs 1 and 2). These data demonstrate the relevance of our findings for the human disease. These results also indicate that PSs are likely to play a role in ER Ca^{2+} leak in lymphoblasts. It has been previously reported that deletion of presenilins in B cell lymphocytes results in deficits in both lipopolysaccharide and B-cell antigen receptor-induced proliferation and signal transduction events, including a deficit in anti-IgM-mediated Ca^{2+} influx [39]. A possible explanation is that the impaired store-operated Ca^{2+} influx in PS DKO lymphoblasts [39] is related to loss of ER Ca^{2+} leak function due to genetic deletion of presenilins in these cells.

In our experiments the Ca^{2+} signaling defects were restricted to FAD lymphoblasts with PS1 and PS2 mutations and were not observed in lymphoblasts from YAD1 and YAD2 AD patients without identified genetic mutations or from patients harboring FTDP17 mutation Tau-R406W (Fig. 2). There was an increase in the ER Ca^{2+} pool in lymphoblasts from the AβPP-V717L FAD patient and lymphoblasts from the OAD AD patient without identified genetic mutation, but the changes did not reach the level of statistical significance (Fig. 2). Additional experiments with AβPP-FAD mutations may help to clarify the effects of AβPP mutations on Ca^{2+} signaling. The heterogeneity in Ca^{2+} signaling for the fibroblasts from sporadic AD patients has been reported previously [40]. Overall, our studies with these samples indicate that Ca^{2+} signaling defects in human lymphoblasts are specifically and robustly linked with certain FAD PS mutations (Fig. 2). These conclusions have been confirmed in rescue experiments with PS1-FAD constructs expressed in PS DKO MEF cells (Fig. 3).

Not all FAD mutations in PSs resulted in overloaded ER Ca^{2+} pool and loss of ER Ca^{2+} leak function. In our combined Ca^{2+} imaging studies ([21, 22] and in the present report) we tested 23 FAD mutations in PS1, 1 FAD mutation in PS2 and 3 FTD-implicated PS1 mutations (Table 1). We concluded that 14 FAD mutations (M139V, M146I/V/L, L166P, G217D, K239E, A246E, V261F, E273A, G384A, L420R, A426P, A431E, P436Q mutations in PS1, and N141I/L mutation in PS2) abolished ER Ca^{2+} leak function of presenilins (Table 1, Fig. 5). These conclu-

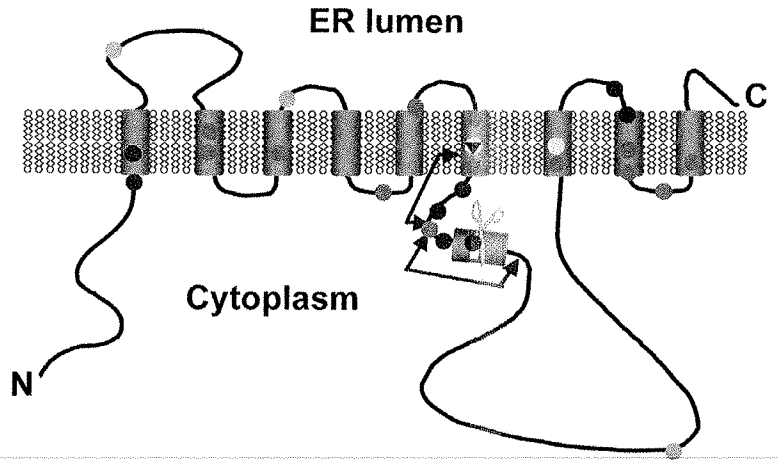

Fig. 5. Schematic representation of PS1-FAD mutations analyzed in ER Ca^{2+} leak function experiments. Molecular model of presenilins [8, 9]. The nine transmembrane domains (TM1-TM9) of presenilins, the γ-secretase catalytic aspartate residues (D257 and D385, yellow) and the site of the endoproteolytic cleavage of presenilins are shown. The positions of PS1 FAD mutants L85P, M139V, G217D, K239E, V261F, P264L, R269G, ΔE8, A426P, A431E, T291P, N405S, C410Y, and L420R examined in our study are shown. Also shown are positions of A79V, M146V, PS2-N141I, L166P, A246E, D257A, ΔE9, E273A, G384A, P436Q mutations analyzed in the previous studies [21,22]. The positions of PS1 FTD-implicated mutants L113P, G183V, and Rins352 analyzed in the previous study [22] are also shown (light blue color). The effects of FAD mutations on ER Ca^{2+} leak activity of presenilins is color coded – red color is used for LOF mutations, blue color is used for "functional" mutations. (Colours are visible in the electronic version of the article at www.iospress.nl.)

sions are based on the lack of channel activity in planar bilayers with recombinant presenilins and by failure of these mutants to rescue Ca^{2+} signaling defects in PS DKO MEF cells. In contrast, another 10 FAD mutations in PS1 (A79V, L85P, P264L, R269G, ΔE8, E280G, ΔE9, T291P, N405S, and C410Y) appeared to be functional in our experiments (Table 1, Fig. 5). The PS1-ΔE9 FAD mutant acted as a "gain of function" mutant based on bilayer experiments [21]. Other PS1 mutants were able to rescue Ca^{2+} signaling defects in PS DKO MEF cells but were not tested in bilayers. These mutants may correspond to a gain of function, normal function, or partial loss of function mutations and were classified as "functional" (Table 1). Interestingly, PS1-ΔE9 and most other "functional" PS1-FAD mutants (L85P, P264L, R269G, ΔE8, E280G, T291P, N405S, and C410Y) segregated with the CWP pathology and/or SP clinical phenotype (Table 1). The only exception is A79V mutation which has not been previously linked with CWP/SP phenotype. It is interesting that a highly variable age of FAD onset and incomplete penetrance was observed in families which carry the A79V mutation [41]. Also, the mean age of disease onset in PS1-A79V pedigrees was 61, which is 20 years older than most other PS1-FAD mutations (Table 1). All 3 PS1 mutants implicated in FTD (L113P, G183V, and Rins352) were functional in ER Ca^{2+} leak assay (Table 1). The Rins352 mutation is probably not pathogenic as the same patient also has a mutation in progranulin, which is most likely responsible for the disease [42]. The pathogenic status of the L113P and G183V mutations remains to be elucidated.

As a result of the analysis of ER Ca^{2+} leak pathway activity we were able to divide FAD PS1 mutations in "loss of function" (LOF) and "functional" groups (Table 1). The LOF mutations are spread out through the sequence of PS1 (within exons 5, 6, 7, 8, 11, and 12 of PSEN1 gene) and are mostly localized to the transmembrane domains (Fig. 5, Table 1). Most "functional" PS1 FAD mutations are concentrated in the initial portion of a large HL6 cytosolic loop between TM6 and TM7 (Fig. 5), the region encoded by exons 8 and 9 of the PSEN1 gene (Table 1). Remarkably, all "functional" mutations are associated with CWP/SP phenotype and

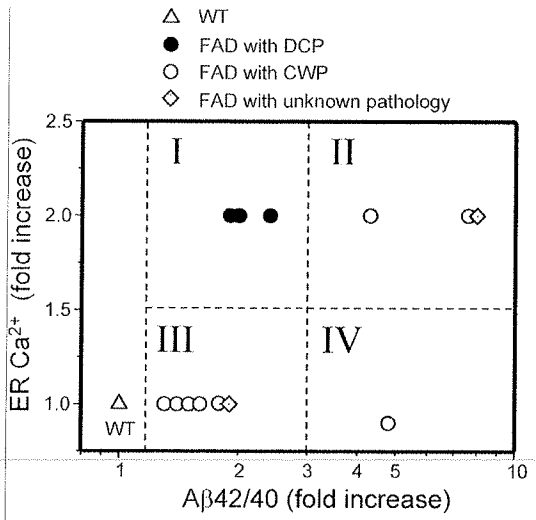

Fig. 6. Effects of PS1-FAD mutations on ER Ca^{2+} levels and $A\beta_{42/40}$ ratios. For each PS1-FAD mutant the $A\beta_{42/40}$ ratios and ER Ca^{2+} levels were normalized to the corresponding values for the WT (open triangle). The PS1-FAD mutants with confirmed DCP pathology (M139V, M146L, A246E) are plotted as solid circles. The PS1-FAD mutants with confirmed CWP pathology (L166P, P436Q, P264L, ΔE8, E280G, ΔE9, T291P, C410Y) are plotted as open circles. The PS1-FAD mutants with unknown pathology (G384A, L85P) are plotted as open diamonds. For mutants with LOF of ER Ca^{2+} leak pathway the ER Ca^{2+} levels assumed to be increased 2-fold. For "functional" mutants the ER Ca^{2+} levels assumed to be unchanged. The fold increase in $A\beta_{42/40}$ ratio for each of the PS1 FAD mutants was obtained from on-line database http://www.molgen.ua.ac.be/ADMutations [43]. The diagram divided into 4 quadrants (I, II, III, IV) as shown.

none of the "functional" mutations led to typical DCP AD pathology (Table 1). To explain these results we propose that the disruption of both ER Ca^{2+} leak and γ-secretase function of PS1 causes pathological changes in the brains of PS1-FAD patients. To represent these ideas quantitatively, we plotted the increase in $A\beta_{42/40}$ ratio against the increase in ER Ca^{2+} levels for each of the PS1-FAD mutants (Fig. 6). The fold increase values for $A\beta_{42/40}$ ratios (Table 1, Fig. 6) for each of the PS1 FAD mutants were extracted from the on-line database http://www.molgen.ua.ac.be/ADMutations [43]. The change in ER Ca^{2+} levels was plotted based on our studies of ER Ca^{2+} leak activity (Table 1). We made an assumption that for LOF mutants the ER Ca^{2+} levels were increased 2-fold, for "functional" mutants the ER Ca^{2+} levels were unchanged, and for the GOF mutant PS1-ΔE9 the ER Ca^{2+} levels were reduced by 10%. The $A\beta_{42/40}$ ratios and ER Ca^{2+} levels were normalized to the corresponding values for the WT (open triangle). The 3 PS1-FAD mutants with confirmed DCP pathology (M139V, M146L, A246E) [31, 44,45] were plotted as solid circles, the 8 PS1-FAD mutants with confirmed CWP pathology (L166P, P436Q, P264L, ΔE8, E280G, ΔE9, T291P, C410Y) [13–15] were plotted as open circles, and the 2 PS1-FAD mutants with unknown pathology (G384A, L85P) were plotted as diamonds. For the remaining 9 PS1-FAD mutants (G217D, K239E, V261F, E273A, L420R, A426P, A431E, R269G, and N405S) $A\beta_{42/40}$ values were not available and these mutants could not yet be plotted. The late-onset, partially-penetrant PS1-A79V mutation and PS2-N141I mutation were not plotted.

The resulting diagram can be divided into 4 quadrants (Fig. 6): quadrant I (high ER Ca^{2+}, small increase in $A\beta_{42/40}$), quadrant II (high ER Ca^{2+}, large increase in $A\beta_{42/40}$), quadrant III (low ER Ca^{2+}, small increase in $A\beta_{42/40}$), quadrant IV (low ER Ca^{2+}, large increase in $A\beta_{42/40}$). Interestingly, all 3 mutations with confirmed DCP are located in quadrant I, and all mutations with confirmed CWP are located in quadrants II, III, or IV (Fig. 6). To explain these results we propose that both ER Ca^{2+} dyshomeostasis and increase in $A\beta_{42/40}$ ratios can play a role in development of AD pathology. If the pathology is driven by both ER Ca^{2+} overload and an increase in $A\beta_{42/40}$ ratios, then the formation of DCP is favored, as it is the case for mutations in quadrant I (M139V, M146L, A246E). However, if the pathology is primarily driven by an increase in the $A\beta_{42/40}$ ratio, then the formation of $A\beta_{42}$-enriched CWP plaques is strongly favored. We propose that this situation can occur when ER Ca^{2+} levels are not affected (quadrant III) or when ER Ca^{2+} levels are affected but an increase in $A\beta_{42/40}$ ratios is large (quadrant II). The extreme case of this situation is quadrant IV, which corresponds to both low ER Ca^{2+} levels and large increase in $A\beta_{42/40}$ ratios (Fig. 6). Indeed, the only mutation located in quadrant IV (PS1-ΔE9) results in the most robust and penetrant CWP/SP clinical phenotype [28,29]. The proposed classification has a predictive power. For example, we predict that mutations G384A (located in quadrant II) and L85P (located in quadrant III) should also be linked with CWP pathology. It will be of interest to test this prediction experimentally. Although the pathological evaluation of these mutants has not yet been reported, the SP clinical phenotype has been previously described for PS1-L85P patients [32], consistent with our predictions.

The proposed hypothesis provides a novel insight into the relative contributions of Ca^{2+}-driven and amyloid-driven pathological pathways in AD patients. We would like to propose that if pathology is primari-

ly driven by an increase in $A\beta_{42/40}$ ratio, then formation of $A\beta_{42}$-enriched CWP plaques is favored. It has been previously proposed that only mutations that cause large increases in $A\beta_{42/40}$ ratios, such as PS1ΔE9 and PS1-436Q, can lead to CWP plaques [16]. At some level our proposal can be considered as expansion of the same idea which now adds "Ca^{2+} dimension" to the "amyloid dimension". In agreement with the earlier proposal [16], we argue that PS1-FAD mutations linked with large increases in $A\beta_{42/40}$ ratio should yield CWP phenotype independently from effects of the same mutation on ER Ca^{2+} leak (quadrants II and IV on Fig. 6). However, even PS1 mutations that have relatively small effects on $A\beta_{42/40}$ ratios would yield CWP phenotype if ER Ca^{2+} leak is not effected (quadrant III on Fig. 6). On another hand, if pathology is driven by both Ca^{2+} dyshomeostasis and relatively modest increase in the $A\beta_{42/40}$ ratio, then dense core or "diffuse" plaques are favored (quadrant I). It is possible that the relative contribution of these pathways may vary in different members of the same pedigree, resulting in a variable presentation of CWP/SP phenotype in most cases [13–15]. In agreement with this idea, the most robust CWP/SP phenotype was reported for PS1-ΔE9 mutant [28,29], which has the largest effect on γ-secretase activity and acts as a "gain of function" mutant for ER Ca^{2+} leak channels (quadrant IV, Fig. 6). Our hypothesis indeed predicts that the mutant with these properties should shift the balance as far as possible towards pure amyloid-driven pathology and formation of CWP plaques.

So far our studies have been focused on PS1-FAD cases, but similar ideas may also apply to understanding sporadic AD as well. Some of sporadic AD patients also present CWP pathology [46], suggesting that CWP are not specific for early-onset FAD resulting from PS1 mutations. It is possible that the relative contribution of "Ca^{2+}-driven" and "amyloid-driven" pathogenic processes may vary between different brain regions, resulting in different abundance of CWP and DCP plaques in different areas of the brain for sporadic and familial AD patients. Future studies will be needed to test the proposed hypothesis and to relate our findings to understanding the pathogenesis of familial and sporadic AD.

ACKNOWLEDGMENTS

We thank Leah Benson for administrative assistance and Sam Gandy (Mount Sinai School of Medicine, NYC) for providing us with PS1-ΔE8 construct, Bart De Strooper (KU Leuven) for providing us with PS DKO MEF cells, Kelly Michelle Faber (National Cell Repository for AD) and Dwight German for comments on the manuscript. Samples from the National Cell Repository for Alzheimer's Disease (NCRAD), which receives government support under a cooperative agreement grant (U24 AG21886) awarded by the National Institute on Aging (NIA), were used in this study. We thank contributors, including the Alzheimer's Disease Centers who collected samples used in this study, as well as patients and their families, whose help and participation made this work possible. Ilya Bezprozvanny is a holder of Carla Cocke Francis Professorship in Alzheimer's Research and supported by NIA R01AG030746, the Alzheimer's Association Research Grant IIRG-06-24703, McKnight Neuroscience of Brain Disorders Award and the King Foundation award. Omar Nelson was supported by the Division of Basic Science Training grant and NIH predoctoral Fellowship award for Minority students (F31).

Authors' disclosures available online (http://www.j-alz.com/disclosures/view.php?id=416).

REFERENCES

[1] Hardy J (2009) The amyloid hypothesis for Alzheimer's disease: a critical reappraisal. *J Neurochem* **110**, 1129-1134.

[2] Hardy J, Selkoe DJ (2002) The amyloid hypothesis of Alzheimer's disease: progress and problems on the road to therapeutics. *Science* **297**, 353-356.

[3] Small SA, Duff K (2008) Linking Abeta and tau in late-onset Alzheimer's disease: a dual pathway hypothesis. *Neuron* **60**, 534-542.

[4] Bertram L, Tanzi RE (2008) Thirty years of Alzheimer's disease genetics: the implications of systematic meta-analyses. *Nat Rev Neurosci* **9**, 768-778.

[5] Bergmans BA, De Strooper B (2010) gamma-secretases: from cell biology to therapeutic strategies. *Lancet Neurol* **9**, 215-226.

[6] Hutton M, Lendon CL, Rizzu P, Baker M, Froelich S, Houlden H, Pickering-Brown S, Chakraverty S, Isaacs A, Grover A, Hackett J, Adamson J, Lincoln S, Dickson D, Davies P, Petersen RC, Stevens M, de Graaff E, Wauters E, van Baren J, Hillebrand M, Joosse M, Kwon JM, Nowotny P, Che LK, Norton J, Morris JC, Reed LA, Trojanowski J, Basun H, Lannfelt L, Neystat M, Fahn S, Dark F, Tannenberg T, Dodd PR, Hayward N, Kwok JB, Schofield PR, Andreadis A, Snowden J, Craufurd D, Neary D, Owen F, Oostra BA, Hardy J, Goate A, van Swieten J, Mann D, Lynch T, Heutink P (1998) Association of missense and 5'-splice-site mutations in tau with the inherited dementia FTDP-17. *Nature* **393**, 702-705.

[7] Cruts M, Van Broeckhoven C (2008) Loss of progranulin function in frontotemporal lobar degeneration. *Trends Genet* **24**, 186-194.

[8] Laudon H, Hansson EM, Melen K, Bergman A, Farmery MR, Winblad B, Lendahl U, von Heijne G, Naslund J (2005) A nine-transmembrane domain topology for presenilin 1. *J Biol Chem* **280**, 35352-35360.

[9] Spasic D, Tolia A, Dillen K, Baert V, De Strooper B, Vrijens S, Annaert W (2006) Presenilin-1 maintains a nine-transmembrane topology throughout the secretory pathway. *J Biol Chem* **281**, 26569-26577.

[10] Annaert WG, Levesque L, Craessaerts K, Dierinck I, Snellings G, Westaway D, George-Hyslop PS, Cordell B, Fraser P, De Strooper B (1999) Presenilin 1 controls gamma-secretase processing of amyloid precursor protein in pre-golgi compartments of hippocampal neurons. *J Cell Biol* **147**, 277-294.

[11] De Strooper B, Saftig P, Craessaerts K, Vanderstichele H, Guhde G, Annaert W, Von Figura K, Van Leuven F (1998) Deficiency of presenilin-1 inhibits the normal cleavage of amyloid precursor protein. *Nature* **391**, 387-390.

[12] Wolfe MS, Xia W, Ostaszewski BL, Diehl TS, Kimberly WT, Selkoe DJ (1999) Two transmembrane aspartates in presenilin-1 required for presenilin endoproteolysis and gamma-secretase activity. *Nature***398**, 513-517.

[13] Larner AJ, Doran M (2006) Clinical phenotypic heterogeneity of Alzheimer's disease associated with mutations of the presenilin-1 gene. *J Neurol***253**, 139-158.

[14] Karlstrom H, Brooks WS, Kwok JB, Broe GA, Kril JJ, McCann H, Halliday GM, Schofield PR (2008) Variable phenotype of Alzheimer's disease with spastic paraparesis. *J Neurochem* **104**, 573-583.

[15] Tabira T, Chui DH, Nakayama H, Kuroda S, Shibuya M (2002) Alzheimer's disease with spastic paresis and cotton wool type plaques. *J Neurosci Res* **70**, 367-372.

[16] Houlden H, Baker M, McGowan E, Lewis P, Hutton M, Crook R, Wood NW, Kumar-Singh S, Geddes J, Swash M, Scaravilli F, Holton JL, Lashley T, Tomita T, Hashimoto T, Verkkoniemi A, Kalimo H, Somer M, Paetau A, Martin JJ, Van Broeckhoven C, Golde T, Hardy J, Haltia M, Revesz T (2000) Variant Alzheimer's disease with spastic paraparesis and cotton wool plaques is caused by PS-1 mutations that lead to exceptionally high amyloid-beta concentrations. *Ann Neurol* **48**, 806-808.

[17] Khachaturian ZS (1989) Calcium, membranes, aging, and Alzheimer's disease. Introduction and overview. *Ann N Y Acad Sci* **568**, 1-4.

[18] Bezprozvanny I, Mattson MP (2008) Neuronal calcium mishandling and the pathogenesis of Alzheimer's disease. *Trends Neurosci* **31**, 454-463.

[19] Smith IF, Green KN, LaFerla FM (2005) Calcium dysregulation in Alzheimer's disease: recent advances gained from genetically modified animals. *Cell Calcium* **38**, 427-437.

[20] Ito E, Oka K, Etcheberrigaray R, Nelson TJ, McPhie DL, Tofel-Grehl B, Gibson GE, Alkon DL (1994) Internal Ca2+ mobilization is altered in fibroblasts from patients with Alzheimer disease. *Proc Natl Acad Sci U S A* **91**, 534-538.

[21] Tu H, Nelson O, Bezprozvanny A, Wang Z, Lee S-F, Hao YH, Serneels L, De Strooper B, Yu G, Bezprozvanny I (2006) Presenilins form ER calcium leak channels, a function disrupted by mutations linked to familial Alzheimer's disease. *Cell* **126**, 981-993.

[22] Nelson O, Tu H, Lei T, Bentahir M, de Strooper B, Bezprozvanny I (2007) Familial Alzheimer disease-linked mutations specifically disrupt Ca2+ leak function of presenilin 1. *J Clin Invest* **117**, 1230-1239.

[23] Grynkiewicz G, Poenie M, Tsien RY (1985) A new generation of Ca2+ indicators with greatly improved fluorescence properties. *J Biol Chem* **260**, 3440-3450.

[24] Kwok JB, Halliday GM, Brooks WS, Dolios G, Laudon H, Murayama O, Hallupp M, Badenhop RF, Vickers J, Wang R, Naslund J, Takashima A, Gandy SE, Schofield PR (2003) Presenilin-1 mutation L271V results in altered exon 8 splicing and Alzheimer's disease with non-cored plaques and no neuritic dystrophy. *J Biol Chem* **278**, 6748-6754.

[25] Herreman A, Serneels L, Annaert W, Collen D, Schoonjans L, De Strooper B (2000) Total inactivation of gamma-secretase activity in presenilin-deficient embryonic stem cells. *Nat Cell Biol* **2**, 461-462.

[26] Bentahir M, Nyabi O, Verhamme J, Tolia A, Horre K, Wiltfang J, Esselmann H, De Strooper B (2006) Presenilin clinical mutations can affect gamma-secretase activity by different mechanisms. *J Neurochem* **96**, 732-742.

[27] Steiner H, Revesz T, Neumann M, Romig H, Grim MG, Pesold B, Kretzschmar HA, Hardy J, Holton JL, Baumeister R, Houlden H, Haass C (2001) A pathogenic presenilin-1 deletion causes aberrant Abeta 42 production in the absence of congophilic amyloid plaques. *J Biol Chem* **276**, 7233-7239.

[28] Crook R, Verkkoniemi A, Perez-Tur J, Mehta N, Baker M, Houlden H, Farrer M, Hutton M, Lincoln S, Hardy J, Gwinn K, Somer M, Paetau A, Kalimo H, Ylikoski R, Poyhonen M, Kucera S, Haltia M (1998) A variant of Alzheimer's disease with spastic paraparesis and unusual plaques due to deletion of exon 9 of presenilin 1. *Nat Med* **4**, 452-455.

[29] Brooks WS, Kwok JB, Kril JJ, Broe GA, Blumbergs PC, Tannenberg AE, Lamont PJ, Hedges P, Schofield PR (2003) Alzheimer's disease with spastic paraparesis and 'cotton wool' plaques: two pedigrees with PS-1 exon 9 deletions. *Brain* **126**, 783-791.

[30] Jacquemont ML, Campion D, Hahn V, Tallaksen C, Frebourg T, Brice A, Durr A (2002) Spastic paraparesis and atypical dementia caused by PSEN1 mutation (P264L), responsible for Alzheimer's disease. *J Med Genet* **39**, E2.

[31] Haleem K, Lippa CF, Smith TW, Kowa H, Wu J, Iwatsubo T (2007) Presenilin-1 C410Y Alzheimer disease plaques contain synaptic proteins. *Am J Alzheimers Dis Other Demen* **22**, 137-144.

[32] Ataka S, Tomiyama T, Takuma H, Yamashita T, Shimada H, Tsutada T, Kawabata K, Mori H, Miki T (2004) A novel presenilin-1 mutation (Leu85Pro) in early-onset Alzheimer disease with spastic paraparesis. *Arch Neurol* **61**, 1773-1776.

[33] Takao M, Ghetti B, Hayakawa I, Ikeda E, Fukuuchi Y, Miravalle L, Piccardo P, Murrell JR, Glazier BS, Koto A (2002) A novel mutation (G217D) in the Presenilin 1 gene (PSEN1) in a Japanese family: presenile dementia and parkinsonism are associated with cotton wool plaques in the cortex and striatum. *Acta Neuropathol* **104**, 155-170.

[34] O'Riordan S, McMonagle P, Janssen JC, Fox NC, Farrell M, Collinge J, Rossor MN, Hutchinson M (2002) Presenilin-1 mutation (E280G), spastic paraparesis, and cranial MRI white-matter abnormalities. *Neurology* **59**, 1108-1110.

[35] Rogaeva E, Bergeron C, Sato C, Moliaka I, Kawarai T, Toulina A, Song YQ, Kolesnikova T, Orlacchio A, Bernardi G, St George-Hyslop PH (2003) PS1 Alzheimer's disease family with spastic paraplegia: the search for a gene modifier. *Neurology* **61**, 1005-1007.

[36] Dumanchin C, Tournier I, Martin C, Didic M, Belliard S, Carlander B, Rouhart F, Duyckaerts C, Pellissier JF, Latouche JB, Hannequin D, Frebourg T, Tosi M, Campion D (2006) Biological effects of four PSEN1 gene mutations causing Alzheimer disease with spastic paraparesis and cotton wool plaques. *Hum Mutat* **27**, 1063.

[37] Yasuda M, Maeda S, Kawamata T, Tamaoka A, Yamamoto Y, Kuroda S, Maeda K, Tanaka C (2000) Novel presenilin-1 mutation with widespread cortical amyloid deposition but limited cerebral amyloid angiopathy. *J Neurol Neurosurg Psychiatry* **68**, 220-223.

[38] Shrimpton AE, Schelper RL, Linke RP, Hardy J, Crook R, Dickson DW, Ishizawa T, Davis RL (2007) A presenilin 1 mutation (L420R) in a family with early onset Alzheimer disease, seizures and cotton wool plaques, but not spastic paraparesis. *Neuropathology* **27**, 228-232.

[39] Yagi T, Giallourakis C, Mohanty S, Scheidig C, Shen J, Zheng H, Xavier RJ, Shaw AC (2008) Defective signal transduction in B lymphocytes lacking presenilin proteins. *Proc Natl Acad Sci U S A* **105**, 979-984.

[40] Borden LA, Maxfield FR, Goldman JE, Shelanski ML (1992) Resting [Ca2+]i and [Ca2+]i transients are similar in fibroblasts from normal and Alzheimer's donors. *Neurobiol Aging* **13**, 33-38.

[41] Cruts M, van Duijn CM, Backhovens H, Van den Broeck M, Wehnert A, Serneels S, Sherrington R, Hutton M, Hardy J, St George-Hyslop PH, Hofman A, Van Broeckhoven C (1998) Estimation of the genetic contribution of presenilin-1 and -2 mutations in a population-based study of presenile Alzheimer disease. *Hum Mol Genet* **7**, 43-51.

[42] Boeve BF, Baker M, Dickson DW, Parisi JE, Giannini C, Josephs KA, Hutton M, Pickering-Brown SM, Rademakers R, Tang-Wai D, Jack CR, Jr., Kantarci K, Shiung MM, Golde T, Smith GE, Geda YE, Knopman DS, Petersen RC (2006) Frontotemporal dementia and parkinsonism associated with the IVS1+1G->A mutation in progranulin: a clinicopathologic study. *Brain* **129**, 3103-3114.

[43] Cruts M, Van Broeckhoven C (1998) Presenilin mutations in Alzheimer's disease. *Hum Mutat* **11**, 183-190.

[44] Larner AJ, du Plessis DG (2003) Early-onset Alzheimer's disease with presenilin-1 M139V mutation: clinical, neuropsychological and neuropathological study. *Eur J Neurol* **10**, 319-323.

[45] Halliday GM, Song YJ, Lepar G, Brooks WS, Kwok JB, Kersaitis C, Gregory G, Shepherd CE, Rahimi F, Schofield PR, Kril JJ (2005) Pick bodies in a family with presenilin-1 Alzheimer's disease. *Ann Neurol* **57**, 139-143.

[46] Le TV, Crook R, Hardy J, Dickson DW (2001) Cotton wool plaques in non-familial late-onset Alzheimer disease. *J Neuropathol Exp Neurol* **60**, 1051-1061.